

See discussions, stats, and author profiles for this publication at: <https://www.researchgate.net/publication/224808478>

Tuning Nonlinear Optical and Optoelectronic Properties of Vinyl Coupled Triazene Chromophores: A Density Functional Theory and Time-Dependent Density Functional Theory Investigation...

ARTICLE *in* THE JOURNAL OF PHYSICAL CHEMISTRY A · APRIL 2012

Impact Factor: 2.69 · DOI: 10.1021/jp302276w · Source: PubMed

CITATIONS

36

READS

145

4 AUTHORS, INCLUDING:



Vijay Solomon

University of South Carolina

21 PUBLICATIONS 142 CITATIONS

[SEE PROFILE](#)



Veera pandian.p

CEA, University Joseph Fourier - Grenoble 1

2 PUBLICATIONS 40 CITATIONS

[SEE PROFILE](#)



Angeline Vedha

Bishop Heber College

6 PUBLICATIONS 54 CITATIONS

[SEE PROFILE](#)

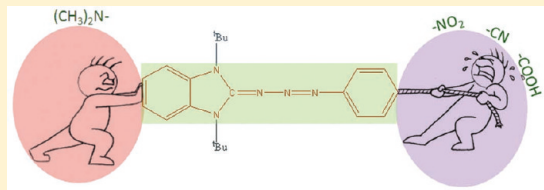
Tuning Nonlinear Optical and Optoelectronic Properties of Vinyl Coupled Triazene Chromophores: A Density Functional Theory and Time-Dependent Density Functional Theory Investigation

R. Vijay Solomon, P. Veerapandian, S. Angeline Vedha, and P. Venuvanalingam*

Theoretical & Computational Chemistry Laboratory, School of Chemistry, Bharathidasan University, Tiruchirappalli-620024, India

Supporting Information

ABSTRACT: Triazenes are a unique class of polyazo compounds containing three consecutive nitrogen atoms in an acyclic arrangement and are promising NLO candidates. In the present work, a series of 15 donor- π -acceptor type vinyl coupled triazene derivatives (VCTDs) with different acceptors ($-\text{NO}_2$, $-\text{CN}$, and $-\text{COOH}$) have been designed, and their structure, nonlinear response, and optoelectronic properties have been studied using density functional theory and time-dependent density functional theory methods. B3LYP/6-311g(d,p) optimized geometries of the designed candidates show delocalization from the acceptor to donor through a π -bridge. Molecular orbital composition analysis reveals that HOMO is stabilized by the π -bridge, whereas acceptors play a major role in the stabilization of LUMO. Among the three acceptors, nitro derivatives are found to be efficient NLO candidates, and tri- and di-substituted cyano and carboxylic acid derivatives also show reasonably good NLO response. The effect of solvation on these properties has been studied using PCM calculations. From TDDFT calculations, the computed absorption spectra of these candidates lie in the range of 350–480 nm in the gas phase and have positive solvatochromism. The ground-state stabilization interactions are accounted from NBO calculations. In an effort to substantiate the thermal stability of the designed candidates, computations have been done to identify the weak interactions in the systems through NCI and AIM analysis. In summary, 10 out of 15 designed candidates are found to have excellent NLO and optoelectronic properties.



1. INTRODUCTION

The design and development of organic nonlinear optical materials have attracted a lot of interest in recent years due to their strong applications in developing optoelectronic devices and modern communication technology.^{1–4} The organic push–pull molecules constituted by an electron donor group (D) connected to an electron acceptor group (A) via a π conjugated bridge are promising NLO candidates with high optical nonlinearity.⁵ In general, the conjugation length, donor (D) and acceptor (A) substitution, solvent environment, and changes in the symmetry of the molecules are the key factors in deciding the NLO response.^{6–10} Numerous D- π -A systems including D/A substituted stilbenes and azoaromatic systems have been investigated.^{11–14} Among the many π conjugated systems, recently synthesized linear $=\text{N}-\text{N}=\text{N}=$ based triazene derivatives attract considerable interest due to their potential NLO applications in semiconductors and nanoelectronics.^{15,16} They have also been used as DNA alkylating agents,¹⁷ photoactive substrates,¹⁸ protecting groups for amines, as well as diazonium salts.^{19,20} Jacquemin et al. have explored the delocalization nature of these triazenes,²¹ whereas Stamboliyska and co-worker have quantified their push–pull character.²² Recently, Tozer et al. have investigated the functional assessment of these triazenes.²³ This has been the motivation for the present work wherein triazenes are examined as candidates with better NLO performance using DFT/TDDFT calculations. The objective of the present work is to

systematically investigate and understand the electronic properties of vinyl fused triazene derivatives with $-\text{NO}_2$, $-\text{CN}$, and $-\text{COOH}$ as their acceptors (A) and determine its appropriate positioning in these triazene derivatives for better NLO response. Throughout this study, the $-\text{N}(\text{CH}_3)_2$ group is used as the donor. Natural bond orbital analysis (NBO), noncovalent interaction (NCI) analysis, and topological analysis (AIM) have been carried out for a deeper understanding of the factors that contribute to their NLO response. The effects of solvent on the dipole moment, absorption, and NLO properties of these designed molecules are also investigated using PCM calculations.

2. COMPUTATIONAL DETAILS

The structures of various vinyl coupled triazene derivatives (VCTDs) chosen for the work are shown in Figure 1. B3LYP^{24,25} functional is found to perform well for most of the organic molecules, and therefore the same is adopted here.^{22,26} The geometries of the molecules in their ground state have been optimized using the hybrid exchange-correlation B3LYP functional with the 6-311g(d,p) basis set. Stationary points located have been characterized by computing vibra-

Received: March 8, 2012

Revised: April 11, 2012

Published: April 20, 2012

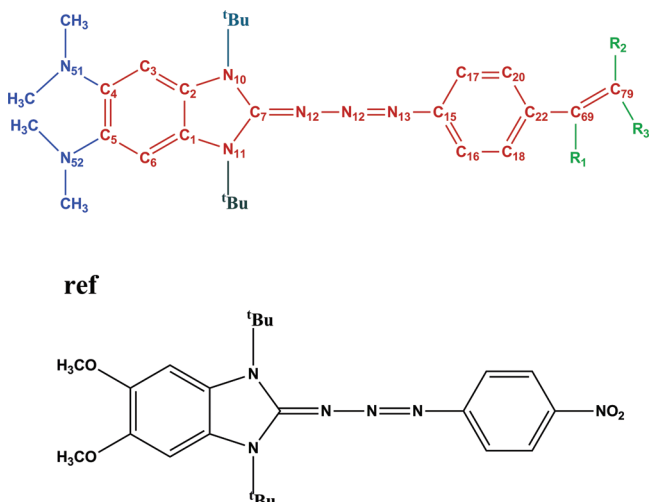


Figure 1. The structures of designed VCTDs.

tional frequencies, and all geometries are found to be minimum energy structures. First-order hyperpolarizability, the measure of NLO response of the material, is calculated.

As reported earlier,²⁷ the first-order hyperpolarizability has been calculated at 6-311g(d,p) level. From this β_{tot} , a scalar quantity can be computed from the x , y , and z components of β using eq 1.

$$\beta_{\text{tot}} = (\beta_x^2 + \beta_y^2 + \beta_z^2)^{1/2} \quad (1)$$

where

$$\beta_x^2 = (\beta_{xxx} + \beta_{xyy} + \beta_{xzz})^2 \quad (2)$$

$$\beta_y^2 = (\beta_{yyy} + \beta_{yzz} + \beta_{yxz})^2 \quad (3)$$

$$\beta_z^2 = (\beta_{zzz} + \beta_{zxz} + \beta_{zyy})^2 \quad (4)$$

Time-dependent density functional theory (TDDFT)²⁸ has been employed here to calculate the vertical excitation energy, absorption wavelength, and oscillator strength on the ground-state optimized geometries at 6-311g(2d,p) level.²⁹ The polarizable continuum model (PCM) has been used to examine the solvent effect on the calculated properties of the species.³⁰

Further, natural bond orbital analysis (NBO)^{31,32} has been carried out at B3LYP/6-311(d,p) level to analyze the stabilizing interactions of these molecules. To gain further insights into the bonding nature of these triazene derivatives and the impact of electron-withdrawing substituents, topological analysis has been performed using the AIM 2000 package,³³ and the corresponding wave function has been generated at B3LYP/6-311g(d) level. Further noncovalent interaction (NCI)³⁴ analysis has been done to shed light on the nonbonding interactions. All of the calculations have been carried out using the Gaussian 03 and Gaussian 09 suites of programs.³⁵

3. RESULTS AND DISCUSSION

A total of 15 molecules (VCTDs) have been chosen (Figure 1), and all of them are asymmetric D- π -A push-pull molecules (C_1). They fall into three groups, nitro (1a–1e), cyano (2a–2e), and carboxylic acid (3a–3e) substituted VCTDs, where “a” denotes trisubstituted derivatives, “b” and “c” are disubstituted, and “d” and “e” are monosubstituted derivatives. The best triazene with better NLO response reported so far is

taken as reference (ref) and comparisons were made using the new candidates here.¹⁶

3.1. Ground-State Geometries. The selected B3LYP/6-311g(d,p) optimized geometrical parameters are given in SIT1, and the data show that these molecules are not completely flat but are slightly twisted as reported earlier²² ($C_7-N_2-N_3-N_4 < 3^\circ$), and the π -electrons are evenly delocalized through the triazeno linkage and benzene rings, making them as dynamic D- π -A push-pull molecules. All proposed structures are found to have a $N-N-N$ angle around 116° and a dihedral angle ($N_{12}-N_{13}-N_{14}-C_{15}$) of 179° , indicating planarity of the molecules (Table SIT1).

Among the disubstituted derivatives, especially disubstitution in positions 1 and 2, the vinyl moiety and the benzene ring are not in-plane as indicated by a dihedral angle of 35° . Therefore, it hinders the effective π conjugation and is higher in energy as compared to derivatives with disubstitution at 2,2 position by ~ 2 kcal/mol. Therefore, in all of the cases, the molecules 1c, 2c, and 3c are more stable than 1b, 2b, and 3b, respectively. At the same time, the mutual pulling of electrons of vinylic π bond from both ends leads to the stabilization of the π bond. In monosubstituted VCTDs, substitution at C69 leads to better stabilization than that at C79, presumably due to extended conjugation, and hence the order of stability in monosubstituted VCTDs is d > e. It is also interesting to note that all of the N–N and C–N bond lengths are well placed between N=N and C=N bond length ranges (Figure 2), whereas C–C

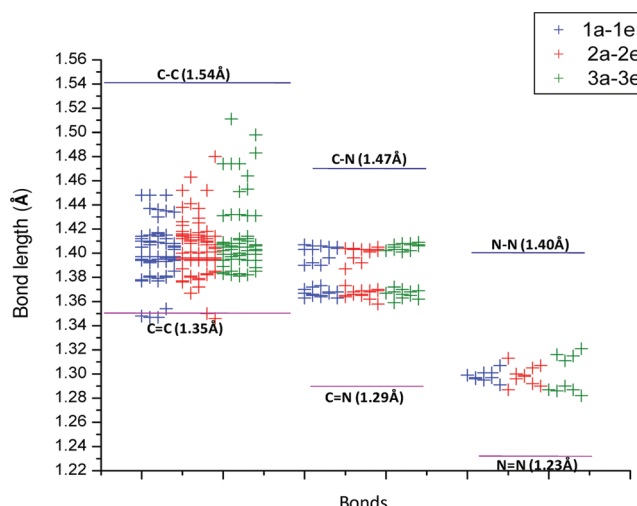


Figure 2. Illustration of π delocalization from calculated C–C, C–N, and N–N bond lengths at B3LYP/6-311g(d,p) level.

bond lengths in (1a–1e) molecules exhibit higher double bond character than in 2a–2e and 3a–3e. We presume that the vinyl substitution has increased the π -conjugation significantly; for instance, the reference molecule has a longer N–N bond (1.27–1.33 Å) as compared to the proposed candidates whose N–N bond lengths fall in the range 1.26–1.32 Å. This shows that all of the C–C, N–N, and N–C bonds in the spacer including triazeno linkage have partial double bond character as shown in Figure 2. This supports the excellent π conjugation observed in these molecules. The calculation of the bond ellipticity (ε), which is defined as $(\lambda_1/\lambda_2) - 1$ through the AIM approach, also provides quantitative evidence for the π bond character of a molecule. When $\varepsilon \rightarrow 0$, the bond belongs to a typical σ bond, and the larger is the ε value, the stronger will be

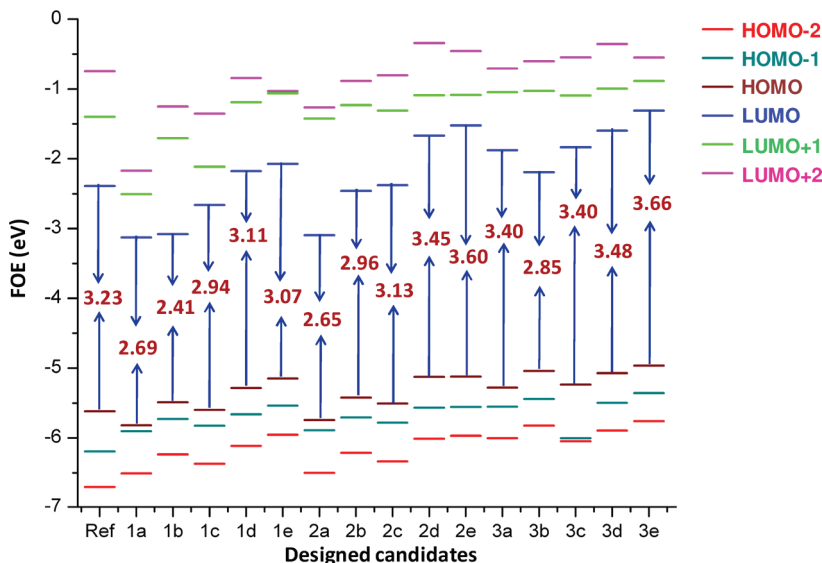


Figure 3. Molecular orbital energy level diagram of designed VCTDs.

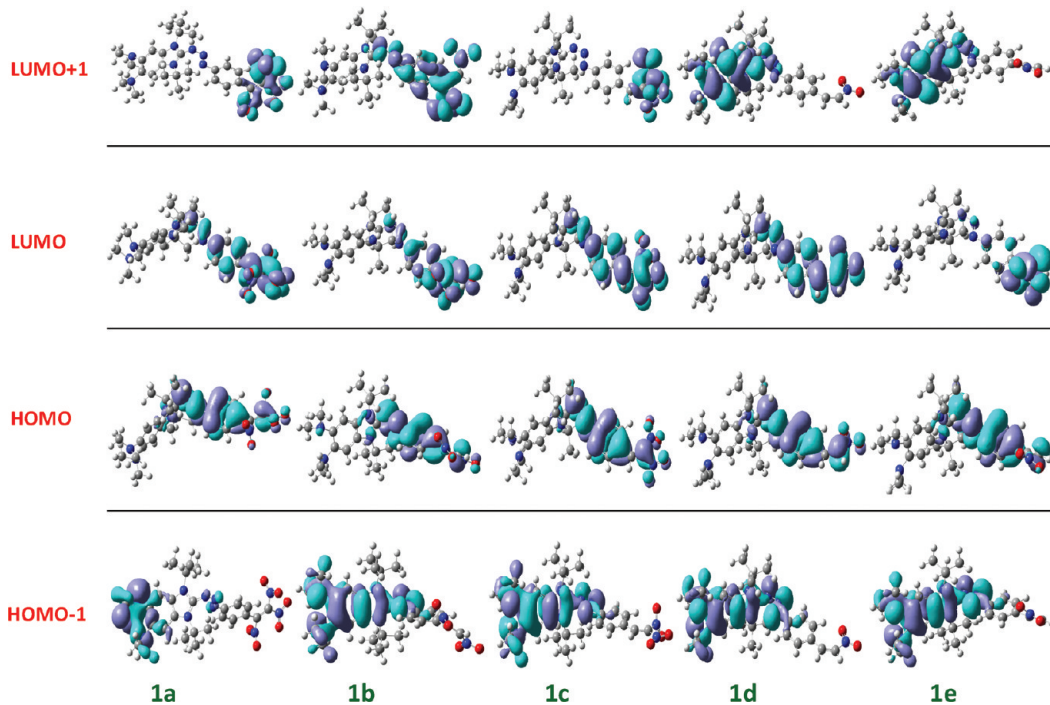


Figure 4. Frontier molecular orbitals of nitro VCTDs.

the π character. The calculated ellipticity values (SIT2) indicate the existence of delocalization of π bond throughout the molecule, which has been also observed from the calculated bond parameters.

Bielawski et al. reported that triazene containing *N*-methyl groups is less stable than that of *N*-*tert*-butyl substituted derivatives.¹⁶ This poses a question as to why the *N*-isobutyl group gives stabilization to the molecules. AIM analysis throws light on this issue, and interestingly these molecules show noncovalent interactions between the *N*-*tert*-butyl moiety and triazeno linkage that cause thermal stability, which will be discussed in detail in section 3.8.

3.2. Frontier Molecular Orbital Analysis. The chemical reactivity and kinetic stability of a molecule are often characterized using frontier molecular orbitals, and it is also

used to obtain qualitative information about the optical and electrical properties of molecules. Moreover, the HOMO–LUMO energy gap (optical gap) is used to understand the charge transfer interaction that occurs within a molecule. The combined molecular orbital energy level graph constituted by LUMO+1 to HOMO–1 for all 15 molecules is given in Figure 3.

It may be noted that the LUMO is progressively stabilized as $1\mathbf{a} > 1\mathbf{b} > 1\mathbf{c} > 1\mathbf{d} > 1\mathbf{e}$, but the order of reactivity in nitro VCTDs is $1\mathbf{b} > 1\mathbf{a} > 1\mathbf{c} > 1\mathbf{d} > 1\mathbf{e}$. The competitive electron pulling nature of the nitro group and pushing nature of the dimethyl amine group result in dynamic delocalization of π electrons throughout the molecule. Figure 4 represents the frontier molecular orbitals of nitro VCTDs. From that it is clear that the electronic distribution of the HOMO is delocalized

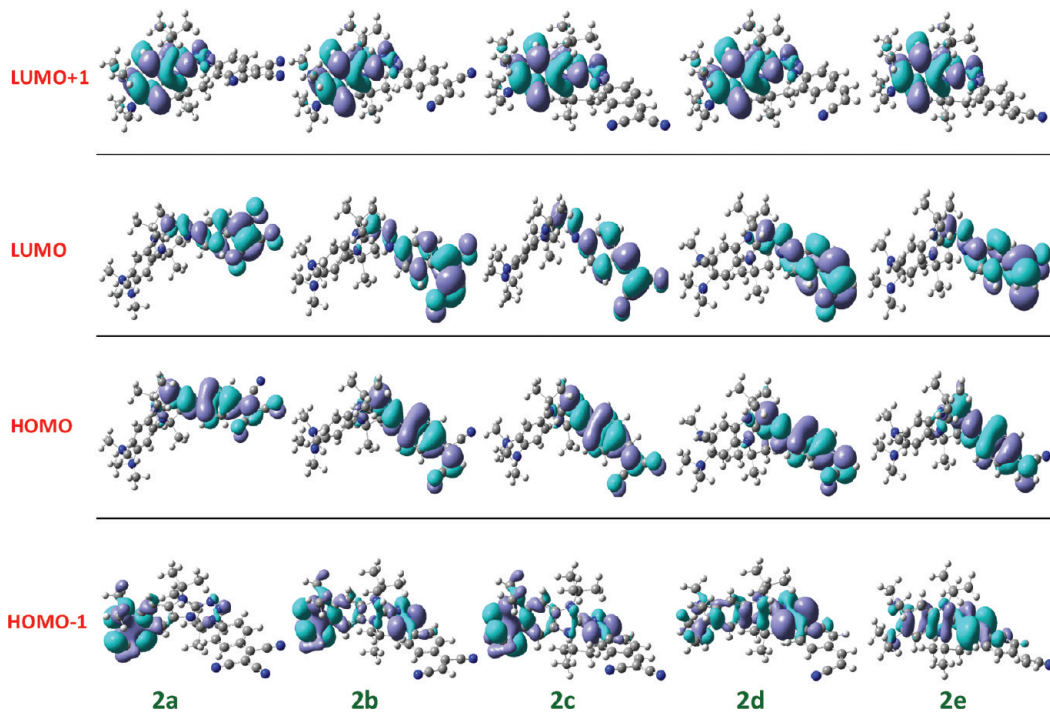


Figure 5. Frontier molecular orbitals of cyano VCTDs.

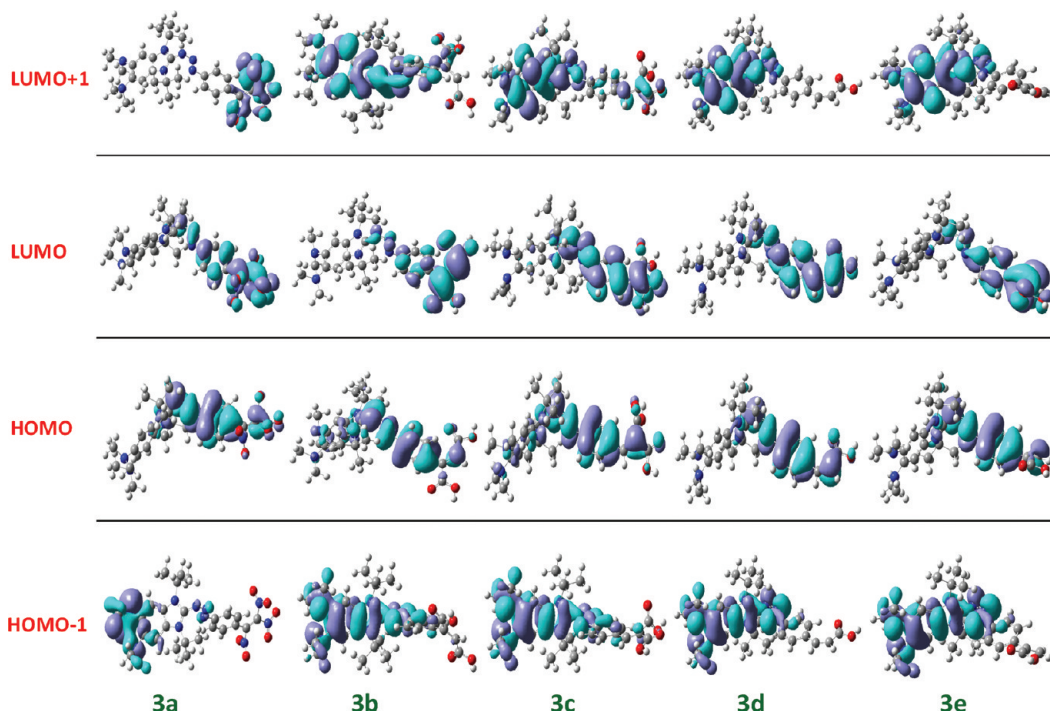


Figure 6. Frontier molecular orbitals of carboxylic acid VCTDs.

over the triazeno linkage and benzene ring, whereas the LUMO is mainly constituted by the acceptor moieties.

The frontier molecular orbitals of cyano VCTDs (**2a–2e**) are given in Figure 5. It shows that HOMO mainly lies on the triazeno linkage and benzene ring as observed in nitro derivatives, and the major contribution to LUMO is from the vinylic part. Yet HOMO-1 is mainly localized on the donor and benzimidazole moieties, and minor participation could be seen from triazeno linkage. The energy gap between HOMO

and LUMO is observed to be minimum (2.68 eV) for **2a** and maximum for **2e** (3.63 eV).

As observed in nitro VCTDs, the order of reactivity in carboxylic acid VCTDs is **3b** > **3a** > **3c** > **3d** > **3e**, and their corresponding frontier molecular orbitals are represented in Figure 6. The HOMO-LUMO gap is the lowest for **3b** (2.85 eV), highest for **3e** (3.66 eV), and this indicates **3b** should exhibit better NLO property while **3e** should have a poor NLO character. This is well supported by the facts that the lower is

Table 1. Molecular Orbital Composition (%) in the Ground State for Triazene-Based Derivatives of 1a–3e

| | 1a | | 1b | | 1c | | 1d | | 1e | |
|----------|------|------|------|------|------|------|------|------|------|------|
| | HOMO | LUMO |
| π bridge | 85% | 53% | 90% | 50% | 90% | 57% | 92% | 58% | 94% | 42% |
| butyl | 3% | 1% | 4% | 0% | 3% | 1% | 4% | 1% | 4% | 0% |
| donor | 6% | 0% | 1% | 0% | 1% | 0% | 0% | 0% | 0% | 0% |
| acceptor | 5% | 46% | 5% | 49% | 6% | 41% | 4% | 41% | 2% | 58% |
| | 2a | | 2b | | 2c | | 2d | | 2e | |
| | HOMO | LUMO |
| π bridge | 89% | 76% | 93% | 77% | 89% | 85% | 93% | 87% | 95% | 90% |
| butyl | 3% | 1% | 4% | 1% | 3% | 2% | 3% | 3% | 4% | 3% |
| donor | 1% | 0% | 0% | 0% | 1% | 0% | 0% | 0% | 0% | 0% |
| acceptor | 7% | 23% | 3% | 22% | 7% | 12% | 3% | 9% | 0% | 7% |
| | 3a | | 3b | | 3c | | 3d | | 3e | |
| | HOMO | LUMO |
| π bridge | 92% | 74% | 91% | 65% | 90% | 83% | 93% | 82% | 94% | 78% |
| butyl | 4% | 1% | 3% | 1% | 3% | 3% | 4% | 3% | 4% | 1% |
| donor | 1% | 0% | 2% | 0% | 3% | 0% | 0% | 0% | 0% | 0% |
| acceptor | 3% | 45% | 3% | 35% | 4% | 14% | 3% | 15% | 1% | 20% |

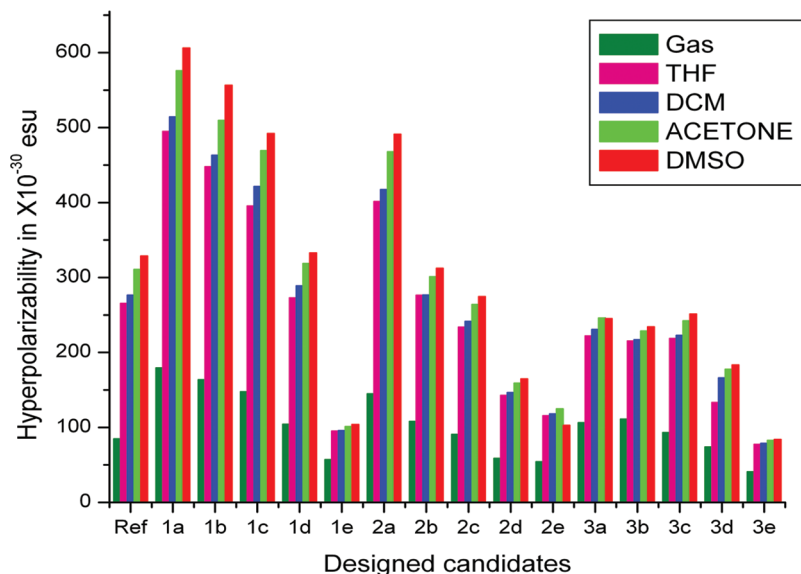


Figure 7. Effect of solvent polarity on first hyperpolarizability for all of the molecules at B3LYP/6-311g(d,p) level.

the optical gap, the greater will be the charge transfer and higher nonlinearity. Generally, it is found that nitro derivatives have the lowest band gap among the three groups considered and the carboxylic acid derivatives have the highest band gap. Out of 15 designed candidates, most of the molecules of nitro and cyano VCTDs exhibit lower optical gap as compared to that of the reference molecule as indicated in Figure 3. Yet in carboxylic acid VCTDs, except for 3b, all other molecules exhibit a higher optical gap.

To get more insight from the frontier orbitals, energetics of the HOMOs and LUMOs of 1a–3e and their corresponding compositions have been calculated using the QMForge program,³⁶ and the data are presented in Table 1.^{37–39} The whole molecule has been segmented as π bridge (benzimidazol, triazene linkage, benzene, and vinyl), donor (dimethylamine), acceptor (−NO₂, −CN, −COOH), and *tert*-butyl groups as indicated in Figure SIF1 (see the Supporting Information). For nitro VCTDs (1a–1e), the contribution of the π bridge is 90–94% to the HOMO level, and other segments like butyl and

acceptor are merely 3–4% and 2–6%, respectively. Donor contribution toward HOMO level is almost 0%. At the same time, different segments contribute differently toward corresponding LUMO. LUMO is equally stabilized by bridge (~50%) and acceptor moiety (~48%) and very minimum contributions from donor and butyl groups.

For cyano VCTDs (2a–2e), the HOMO of 2a is largely stabilized by the contributions from π bridge (~89%) and much less contributions from other segments, whereas contribution of the acceptor group toward LUMO is increased slightly from 7% to 23%, which shows that LUMO is largely contributed by π bridge with a little contribution from acceptor group as observed in nitro VCTDs. In 2e, the HOMO as well as LUMO is mainly contributed by the π bridge (90–95%). It is interesting to note that the donor does not contribute to the HOMO or LUMO. In carboxylic derivatives (3a–3b), HOMO is largely stabilized by the contribution of π bridge (~90%) and less contributions from donor, acceptor, and butyl fragments. Yet the percentage of contributions of π bridge to the LUMO is

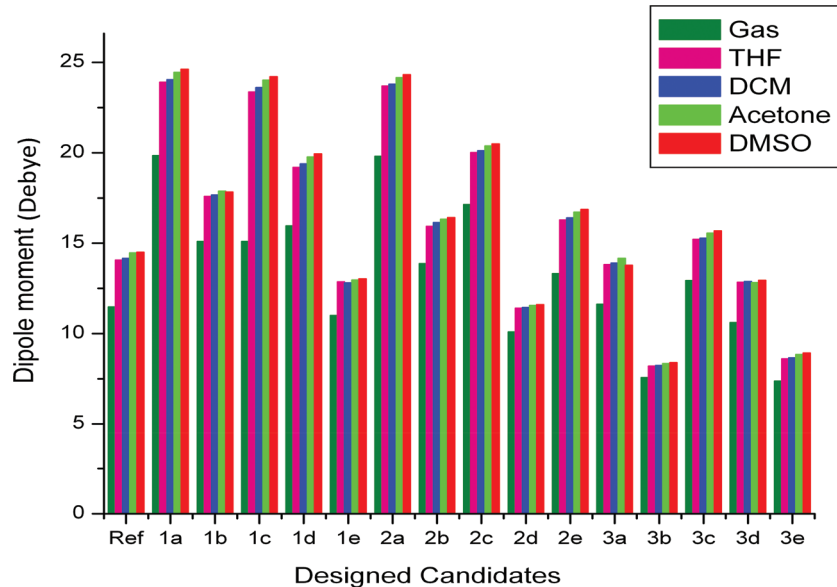


Figure 8. Effect of solvent polarity on dipole moment of all of the molecules at B3LYP/6-311g(d,p) level.

reduced, and the contributions from acceptor are increased moderately, which is not observed in the nitro derivatives. This shows that HOMOs of all of the molecules are largely stabilized by the contributions of π -bridge, whereas the LUMOs are stabilized by both π bridge and acceptor groups. Of all of the substituents, the nitro group stabilizes more as compared to the carboxylic acid group, and very minimum stabilizations are due to cyano substitution. The possibility of extending conjugation to the entire molecule is available only for nitro and carboxylic derivatives but not for the cyano group. In that way, altering the acceptor groups and their position will cause the LUMOs to lower, whereas tuning of HOMOs requires substitution on the π bridge. These results give further clues to a better design of molecules with suitable band gaps.³⁹

3.3. NLO Properties. The nonlinearity of each basic molecular unit of an organic material contributes toward the NLO response of the whole molecule. The NLO activity is characterized by the third rank tensor called first-order hyperpolarizability (β_0). It is well-known that β_0 is described by a $3 \times 3 \times 3$ matrix, and it can be reduced to 10 components from 27 components according to Kleinmann symmetry.⁴⁰ In general, the NLO candidates show asymmetric polarization induced by electron acceptor and electron donor groups in a π conjugated system. It is interesting to analyze and compare the electronic effect on the first-order hyperpolarizability of these triazene derivatives upon substitution of the $-\text{NO}_2$, $-\text{CN}$, and $-\text{COOH}$ groups at appropriate positions in the vinyl moiety. Therefore, in this study, the first-order hyperpolarizability tensor has been calculated for all 15 molecules and is presented in Figure 7.

From Figure 7, it is clear that the magnitude of the first-order hyperpolarizability tensor of molecule **1a** is largest relative to the other molecules. The order of NLO response of nitro VCTDs is **1a** > **1b** > **1c** > **1d** > **1e**. A similar trend has been observed in cyano VCTDs (**2a**–**e**). Yet a higher magnitude of first-order hyperpolarizability tensor has been shown by molecule **3b** as compared to other carboxylic acid VCTDs. This excellently correlates with the optical gap that has been discussed earlier and resembles the observed NLO character. Therefore, the order of NLO response will be **3b** > **3a** > **3c** >

3d > **3e**. The estimated NLO response of these triazene derivatives clearly shows that the greater is the number for electron-withdrawing groups, the greater will be the NLO response ($\text{Na} > \text{Nb} > \text{Nc} > \text{Nd} > \text{Ne}$, $N = 1, 2, 3$). Similarly, the greater is the strength of the electron-withdrawing group, the greater will be the push–pull effect, which in turn results in larger hyperpolarizability values ($1 > 2 > 3$). This study clearly reveals that **1a** shows a 2-fold increase (179.0 esu) in the first-order hyperpolarizability as compared to the reference molecule (80.0 esu). The lowest among the newly designed molecules is **3e** with 40.91 esu. Moreover, all of the tri- and disubstituted triazene derivatives have a greater NLO response than the reference molecule. Except for **1e**, **2d**, **2e**, **3d**, and **3e** molecules, other substituted triazene molecules have been identified as an excellent choice for NLO materials. Thus, these triazene molecules can be tuned upon nitro, cyano, and carboxylic acid substitutions for better NLO performance.

3.4. Effect of Solvation on NLO Response. In general, the polarity of the solvent is said to increase NLO properties,^{41–43} and therefore different solvents with varying polarity have been chosen to study the influence of solvent on the NLO character of these designed molecules. The first-order hyperpolarizabilities are calculated in the presence of solvents such as tetrahydrofuran (THF), dichloromethane (DCM), acetone, and dimethylsulfoxide (DMSO), and the results are summarized in Figure 7. It is implied that an increase in polarity of the solvent increases the first-order hyperpolarizabilities. This can be attributed to the disturbance of the induced field arising from the chromophore on the local field experienced by NLO chromophore.⁴⁴ Similarly, the dipole moment is also largely affected by the solvent medium, which is represented in Figure 8. It shows the dipole moment of these molecules is largely affected upon solvation. An increase in the polarity of the solvent increases the dipole moment.

3.5. Electronic Absorption Spectra in the Gas Phase from TDDFT Calculations. For a molecule to be NLO-active, it has to show good absorption and emission properties, and TDDFT is mainly used to compute excited-state properties.^{45–48} Therefore, TDDFT calculations have been carried out to obtain the electronic vertical singlet excitation energies in the

gas phase. The calculated vertical transition energies (ΔE_{ge}), oscillator strengths (f_0), and the composition and percentage of contributions of various configurations to the excitations are summarized in Table 2.

Table 2. Absorption Maxima (λ_{max} nm), Electronic Transition Energies (ΔE , eV), and Oscillator Strength (f) of 1a–3e in Gaseous State Calculated Using TDDFT Method at the B3LYP/6-311g(2d,p) Level

| molecules | λ_{max} (nm) | oscillator | E (eV) | assignment |
|-----------|-----------------------------|------------|----------|--|
| 1a | 491 | 0.3235 | 2.5267 | HOMO–1→LUMO (46%) |
| 1b | 589 | 0.2751 | 2.1039 | HOMO→LUMO (98%) |
| 1c | 420 | 0.6972 | 2.9497 | HOMO→LUMO (44%) HOMO→LUMO+1 (52%) |
| 1d | 418 | 0.9106 | 2.9639 | HOMO→LUMO (90%) |
| 1e | 333 | 0.6094 | 3.7166 | HOMO→LUMO+2 (41%) |
| 2a | 477 | 0.9649 | 2.6016 | HOMO→LUMO (70%) |
| 2b | 441 | 0.6466 | 2.8131 | HOMO→LUMO (67%) |
| 2c | 410 | 1.2438 | 3.0261 | HOMO→LUMO (90%) |
| 2d | 381 | 0.6936 | 3.256 | HOMO→LUMO (50%) HOMO–2→LUMO (10%) |
| 2e | 376 | 0.4546 | 3.2989 | HOMO→LUMO (53%) |
| 3a | 402 | 0.8298 | 3.0804 | HOMO→LUMO (83%) |
| 3b | 315 | 0.3437 | 3.9272 | HOMO–2→LUMO+1 (25%) HOMO→LUMO+2 (24%) |
| 3c | 405 | 0.7327 | 3.0566 | HOMO→LUMO (57%) HOMO–1→LUMO (15%) |
| 3d | 376 | 0.8593 | 3.2927 | HOMO→LUMO (61%) HOMO–1→LUMO (17%) |
| 3e | 321 | 0.4468 | 3.8577 | HOMO–1→LUMO+1 (68%) |

The nitro VCTDs (1a–1e) show a series of bands between 315 and 600 nm, and in that λ_{max} values of the most intense bands are listed in Table 2. Among them, 1b has the longest

wavelength of absorption (589 nm). This arises due to 98% contributions from HOMO→LUMO. Next to 1b, 1a has an intense band at 491 nm, and this is associated with HOMO–1→LUMO (46%). Molecules 1c and 1d have intense absorption at 420 and 418 nm, respectively. The HOMO→LUMO+2 configurations of 1e contribute 41% to absorption at 333 nm. These absorptions are mainly due to $\pi-\pi^*$ and $n-\pi^*$ transitions. In cyano VCTDs, the most intense band of 2a has the longest wavelength (477 nm) and is mainly contributed by HOMO→LUMO (70%). Among the disubstituted cyano derivates, 2b absorbs slightly at higher wavelength (441 nm) as compared to 2c (410 nm) where both of the transitions are arising from HOMO→LUMO with 67% and 90%, respectively. Similar to nitro VCTDs, 2e has the lowest wavelength of absorption with high excitation energy (3.3 eV).

In carboxylic acid VCTDs, the disubstituted 3c shows slightly longer wavelength of absorption (405 nm) as compared to 3a (402 nm). In both cases, the dominant contributions come from HOMO→LUMO transitions. Surprisingly, 3b has the most intense band at 315 nm, and it is the lowest among all, whereas 3d and 3e show λ_{max} at 376 and 321 nm, respectively. All of these variations in the observed absorption maxima can be directly correlated with the HOMO–LUMO gap [SIT3]. The reference molecule has absorption maxima at 344 nm, whereas all of the designed molecules have absorption shifted to higher wavelength (except 1e, 3b, and 3e). This study reveals that these molecules can be tuned further to have excellent optoelectronic properties.

3.6. Effect of Solvent on UV–Absorption Spectra. To investigate the influence of solvents on the absorption spectral characteristics of the molecules considered here, PCM (B3LYP/6-311g(2d,p)) calculations have been performed on B3LYP/6-311g(d,p) optimized geometries, and the results are presented in Figure 9. The PCM model has been identified as the most successful model for describing solvent effect in DFT and TDDFT calculations.^{49,50} The results of the calculations for

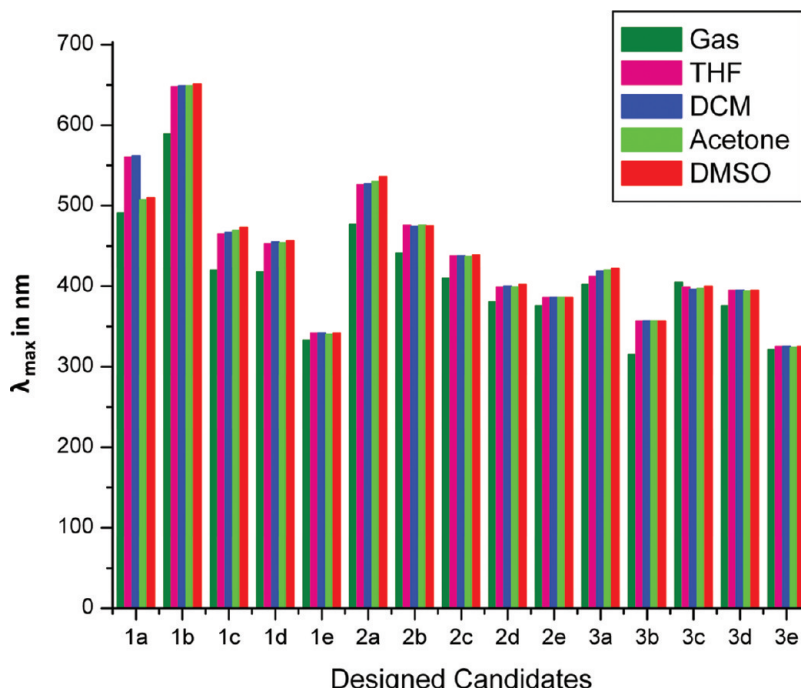


Figure 9. The calculated absorption maxima of all of the designed molecules at B3LYP/6-311g(2d,p).

the 10 lowest lying excited states are predicted for all 15 molecules, and their important excitation wavelengths along with their oscillator strength are listed in SIT4 (see the Supporting Information).

Four different solvents have been used to evaluate the influence of solvent on absorption spectra. The predicted results show that there is a shift in the absorption spectra on solvation. Over all, these molecules show positive solvatochromism. It should be noted that $S_0 \rightarrow S_1$ is the most intense band, whereas excitation to higher singlet states is either partially allowed or forbidden. Further, upon solvation, all excited-state dipole moments increase. For instance, TDDFT calculation shows that **1a** has a dipole moment of 17.3 D in the gas phase, whereas in DMSO, the dipole moment of **1a** is 21.5 D, and this is additional support to the positive solvatochromism. The computed shift in the absorption maxima in solvent phase varies from +4 to +70 nm from the gas phase, while the overall pattern of the absorption maxima remains the same in gas and solvent phases.

3.7. Natural Bond Order Analysis. Because intramolecular interactions such as those between filled and vacant orbitals determine the delocalization in the triazene coupled vinyl chromophores and the extent of delocalization in such D- π -A systems is important in the study of nonlinearity, NBO energy analysis is done to capture such interactions.

To gain further insight into various second-order interactions between filled and vacant orbitals, which is a measure of intramolecular delocalization, natural bond order analysis has been performed at B3LYP/6-311g(d,p), the second-order perturbation energy analysis has been performed to evaluate the donor–acceptor interactions on NBO basis,³² and the results are summarized in SITS.

The computed second-order perturbation analysis clearly shows that the intramolecular hyper conjugative interactions are produced by the orbital overlap between π and π^* , n and π^* , σ and σ^* , and n and σ^* , which causes stabilization of these molecules. Moreover, the n \rightarrow π^* interactions are predominant in **1a**, **1b**, **1c**, and **1d**, whereas in **1e** the interactions between σ (C_7-N_{10}) bond and σ^* (C_7-C_{12}) are favored. Among the 15 molecules, the molecule **3c** possesses $\pi-\pi^*$ interactions, whereas all other cyano and carboxylic acid VCTDs show interactions between the lone pair of nitrogen (N_{11}) and an “empty” orbital of carbon (C_7).

3.8. Implications of Noncovalent Interactions: AIM and NCI Analysis. Besides NLO activity, good thermal stability, solubility, good optical properties, and high hyperpolarizability are important for the design criteria, and they are taken care of.⁴⁵ Noncovalent interactions are important in stabilizing such molecules, and these interactions are analyzed using AIM and NCI analysis. Yang and co-workers have recently introduced noncovalent interactions (NCI) analysis, a new approach based on the analysis of the electron densities and reduced gradients to visualize noncovalant interactions.⁵¹ NCI analysis has been performed on all of the optimized molecules, and gradient isosurfaces for noncovalent interactions of **1a**, **2a**, and **3a** are displayed in Figure 10. (For the remaining molecules, see SIF2.)

NCI depicts the strength of the interactions by color codes; the color of the surface varies from red to blue via green where red signifies strong repulsion, green represents weak interactions, and blue denotes strong attraction. As is evident from Figure 10, all of the molecules possess green isosurface,

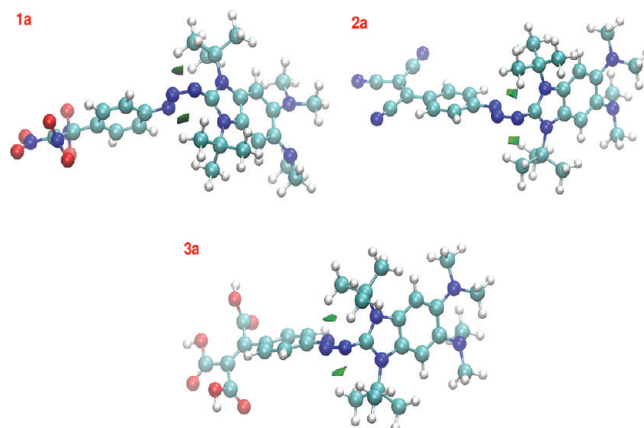


Figure 10. NCI analysis of **1a**, **2a**, and **3a** where the weak interactions are inferred from the green isosurface present between the triazene linkage and the hydrogen of the *N*-tert-butyl group.

thereby exhibiting weak interactions between the triazene linkage and the hydrogen of the *N*-tert-butyl group.

Bielawski et al. reported that the thermogravimetric analysis (TGA) of the triazene molecules with the *N*-tert-butyl group shows higher decomposition temperature than that of its *N*-methyl derivative.¹⁶ Our NCI analysis clearly tells that the weak noncovalent interactions are one of the responsible factors for the stabilization of these candidates and adds further support of their thermal stability.

To draw further insight into the bonding nature of these weak interactions, Bader's atoms in molecules (AIM) theory has been used.^{52,53} In AIM framework, the electron density $\rho(r)$ is used to analyze the bonding and nonbonding interactions present in a chemical system. The strength of the bond is measured with the help of electron density $\rho(r)$ at the BCPs, whereas the nature of the bond is obtained from the Laplacian of electron density $-\nabla^2\rho(r)$.⁵⁴ The presence of a (3,-1) bond critical point (BCP) is accepted as the standard criterion for the existence of bonding and nonbonding interactions.⁵⁵ Figure 11 depicts the molecular graphs corresponding to **1a**, **2a**, and **3a** where the red circle indicates the (3,-1) BCPs and the yellow circle indicates the (3,+1) ring critical point.

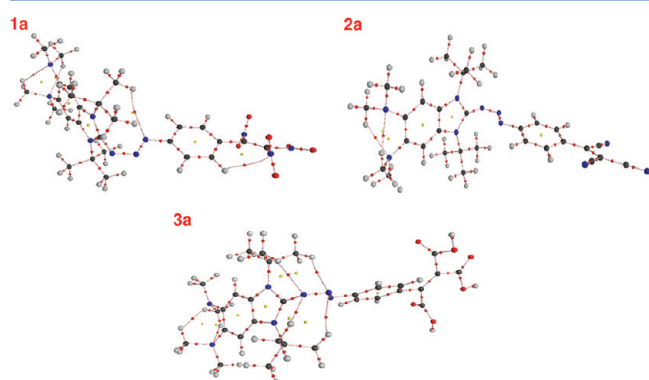


Figure 11. Molecular graphs (set of bond paths and critical points) for **1a**, **2a**, and **3a** are given. Color code for atoms (large balls): carbon (black), hydrogen (gray), nitrogen (blue), and oxygen (red). Color code for critical points (small balls): bond critical points (BCPs, red), ring critical points (RCPs, yellow), and cage critical points (CCPs, green).

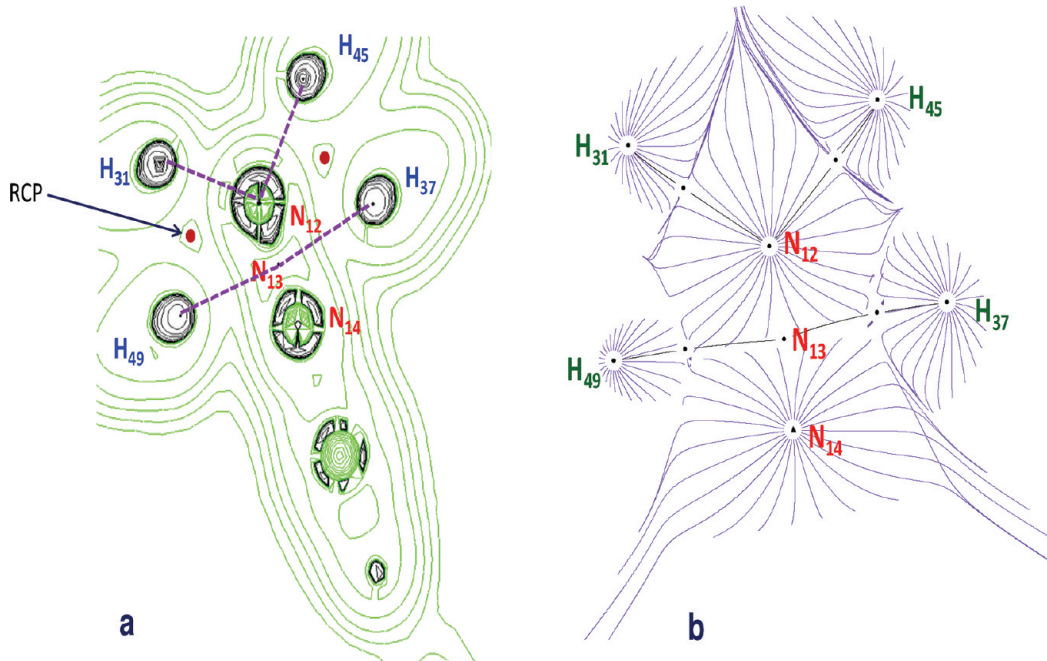


Figure 12. (a) Laplacian of electron density describing the hydrogen-bonding pattern observed in molecule 3a. (b) The gradient vector field trajectories plot describing the presence of hydrogen bonding in molecule 3a.

The NCI analysis shows the presence of weak interactions between the two *N*-*tert*-butyl groups and the triazeno linkage, and AIM further confirms that the weak interactions fall into hydrogen-bond limit through the appearance of a BCP as indicated in the molecular graph. The nitro VCTDs and carboxylic VCTDs show BCP between the triazeno linkage and the *N*-*tert*-butyl group, but the absence of such BCPs in the cyano VCTDs is observed. It can be inferred from the geometries of the cyano VCTDs where the hydrogens of the *N*-*tert*-butyl group and the nitrogen of triazeno linkage are situated at a distance of 3.28 and 3.39 Å and at an angle of $\sim 125^\circ$, which suggests they cannot form hydrogen bond. Yet the other VCTDs show hydrogen bonding where the hydrogens and the interacting nitrogen atoms are in a proper position and orientations in such a way that they can be involved in the hydrogen bonding.

The electron density and Laplacian of ρ of BCPs of interactions in SIT6 reveal that all of the interactions fall into a hydrogen-bond category of 0.002–0.035. It is interesting to note that in molecules 1a and 3a, the triazeno linkage is involved in the hydrogen bonding. 1a shows hydrogen bonds in $N_{12}\cdots H_{50}$, $N_{12}\cdots H_{42}$, $N_{13}\cdots H_{36}$, and $N_{14}\cdots H_{32}$, respectively, as indicated in Figure 11. Thus, N_{12} , N_{13} , and N_{14} of the triazeno linkage are involved in hydrogen bonding with the hydrogen of the *N*-*tert*-butyl group. Apart from this, it also shows other hydrogen bonds among the donor moieties ($-\text{N}(\text{CH}_3)_2$ groups). Similarly, 3a shows triazeno linkage, which is involved in hydrogen bonds ($N_{12}\cdots H_{45}$, $N_{12}\cdots H_{31}$, $N_{13}\cdots H_{37}$, and $N_{13}\cdots H_{49}$) but not with N_{14} . Invariably, in all of the molecules, hydrogen bonds between the two $-\text{N}(\text{CH}_3)_2$ groups are observed. In nitro and carboxylic acid substituted VCTDs (1a–1e and 3a–3e), additional hydrogen bonds are observed between the acceptor moieties (SIF3).

The nature of hydrogen bonds can be clearly explained by monitoring the Laplacian of the electron density map and the gradient vector field trajectories obtained for 3a (Figure 12). It is evident from Figure 12 that the region of electron cloud of

nitrogen is penetrated by hydrogen atoms, and the extent to which each hydrogen atom penetrates triazeno nitrogen's electron cloud indicates that there exist two types of hydrogen bonds (with N_{12} and N_{13}). It is interesting to note that the appearance of the RCP (red circle) resulted from the cyclic nature of electron current further confirms the presence of hydrogen bonding. The gradient vector field trajectories of the electron density of molecule 3a are represented in Figure 12b, and more importantly the gradient vector field trajectories associated with the BCPs define the boundaries of the atoms. It gives a clear picture about how the hydrogen atoms are involved in hydrogen bonding with the N_{13} and N_{12} .

Thus, AIM analysis confirms the intramolecular hydrogen bonding present in these molecules, which largely attributes toward the thermal stability of these *N*-*tert*-butyl substituted triazene derivatives over methyl substituted triazene derivatives. It is clear that the BCPs corresponding to the hydrogen bond observed in AIM analysis can be located in the regions of the isosurface corresponding to stabilizing interactions in nitro and carboxylic acid derivatives. Thus, AIM analysis and NCI analysis are complementing each other in bringing out the noncovalent interactions present in these molecules.

4. CONCLUSIONS

In search of candidates with better NLO response among the triazenes, a comprehensive electronic structure characterization has been performed on 15 newly designed molecules with triazene coupled with vinyl framework, and this further offers useful insights on the design aspects and on the spectral properties. Our results show that the tri nitro VCTD shows excellent NLO performance that is twice good as the best triazene derivatives synthesized so far (ref), and the inclusion of the solvent effect largely affects the first-order hyperpolarizability of the molecule. Moreover, the computed bond parameters show that these molecules have excellent conjugation. The results reveal that molecules 1a–1e, 2a–2c, and 3b are showing lower optical gap than that of the reference

molecule (ref). Frontier molecular orbital analysis reveals that the π -bridge contributes largely to the HOMO, whereas LUMO has equal contribution from the π -bridge and acceptor moieties in almost all of the molecules. TDDFT results show that the coupling vinyl group with triazenes as spacers shifts its λ_{abs} to higher wavelength as compared to that of the corresponding triazene molecule (ref). All of the molecules show positive solvatochromism. NBO analysis offers further insights into intramolecular delocalization. AIM and NCI analysis accounts for the presence of noncovalent interactions and weak hydrogen bonding, which is attributed to the thermal stability of these molecules. As a whole, this investigation provides 10 vinyl coupled triazene-based molecules with better NLO response, which is useful for the synthetic chemist.

■ ASSOCIATED CONTENT

Supporting Information

Optimized geometries of all of the molecules along with their XYZ coordinates, calculated bond parameters, first-order hyperpolarizabilities, TDDFT results, and details of NBO, AIM, and NCI plot analysis. This material is available free of charge via the Internet at <http://pubs.acs.org>.

■ AUTHOR INFORMATION

Corresponding Author

*Tel.: +91 431 2407053. Fax: +91 431 2407045. E-mail: venuvanalingam@yahoo.com.

Notes

The authors declare no competing financial interest.

■ ACKNOWLEDGMENTS

We thank the reviewer for very helpful and suggestive criticism. R.V.S. thanks the University Grants Commission, India, for financial support through the Maulana Azad National Fellowship (ref. no. F.40-17(C/M)/2009(SA-III/MANF)). S.A.V. thanks the University Grants Commission (UGC), India, for FDP program (ref. no. F.ETFTNBD030/FIP-XI PLAN).

■ REFERENCES

- (1) Burland, D. M.; Miller, R. D.; Walsh, C. A. *Chem. Rev.* **1994**, *94*, 31–75.
- (2) Coe, B. J. *Chem.-Eur. J.* **1999**, *5*, 2464–2471.
- (3) Wolff, J. J.; Wortmann, R. *Adv. Phys. Org. Chem.* **1999**, *32*, 121–217.
- (4) Williams, D. J. *Angew. Chem., Int. Ed. Engl.* **1984**, *23*, 690–703.
- (5) Abbotto, A.; Beverina, L.; Bozio, R.; Bradamante, S.; Ferrante, C.; Pagani, G. A.; Signorini, R. *Adv. Mater.* **2000**, *12*, 1963–1967.
- (6) Risser, S. M.; Beratan, D. N.; Marder, S. R. *J. Am. Chem. Soc.* **1993**, *115*, 7719–7728.
- (7) Albert, I. D. L.; Marks, T. J.; Ratner, M. A. *J. Am. Chem. Soc.* **1997**, *119*, 6575–6582.
- (8) Willetts, A.; Rice, J. E. *J. Chem. Phys.* **1993**, *99*, 426–435.
- (9) Di Bella, S.; Marks, T. J.; Ratner, M. A. *J. Am. Chem. Soc.* **1994**, *116*, 4440–4445.
- (10) Meyers, F.; Marder, S.; Pierce, B.; Bredas, J. *J. Am. Chem. Soc.* **1994**, *116*, 10703–10714.
- (11) de la Torre, G.; Vazquez, P.; Agullo-Lopez, F.; Torres, T. *Chem. Rev.* **2004**, *104*, 3723–3750.
- (12) Kanis, D. R.; Ratner, M. A.; Marks, T. J. *Chem. Rev.* **1994**, *94*, 195–242.
- (13) De Boni, L.; Piovesan, E.; Misoguti, L.; Zilio, S.; Mendonca, C. J. *Phys. Chem. A* **2007**, *111*, 6222–6224.
- (14) Breitung, E. M.; Shu, C. F.; McMahon, R. J. *J. Am. Chem. Soc.* **2000**, *122*, 1154–1160.
- (15) Chen, B.; Flatt, A. K.; Jian, H. H.; Hudson, J. L.; Tour, J. M. *Chem. Mater.* **2005**, *17*, 4832–4836.
- (16) Khramov, D. M.; Bielawski, C. W. *J. Org. Chem.* **2007**, *72*, 9407–9417.
- (17) Rouzer, C. A.; Sabourin, M.; Skinner, T. L.; Thompson, E. J.; Wood, T. O.; Chmurny, G. N.; Klose, J. R.; Roman, J. M.; Smith, R. H., Jr.; Michejda, C. J. *Chem. Res. Toxicol.* **1996**, *9*, 172–178.
- (18) Stebani, J.; Nuyken, O.; Lippert, T.; Wokaun, A. *Makromol. Chem. Rapid Commun.* **1993**, *14*, 365–369.
- (19) Gross, M. L.; Blank, D. H.; Welch, W. M. *J. Org. Chem.* **1993**, *58*, 2104–2109.
- (20) Jian, H.; James, M. *J. Org. Chem.* **2005**, *70*, 3396–3424.
- (21) Preat, J.; Michaux, C.; Lewalle, A.; Perpète, E. A.; Jacquemin, D. *Chem. Phys. Lett.* **2008**, *451*, 37–42.
- (22) Kleinpeter, E.; Stamboliyska, B. A. *J. Org. Chem.* **2008**, *73*, 8250–8255.
- (23) Peach, M. J. G.; Le Sueur, C. R.; Ruud, K.; Guillaume, M.; Tozer, D. *J. Phys. Chem. Chem. Phys.* **2009**, *11*, 4465–4470.
- (24) Becke, A. D. *J. Chem. Phys.* **1993**, *98*, 5648–5652.
- (25) Lee, C.; Yang, W.; Parr, R. G. *Phys. Rev. B* **1988**, *37*, 785–789.
- (26) Curtiss, L. A.; Raghavachari, K.; Redfern, P. C.; Pople, J. A. *Chem. Phys. Lett.* **1997**, *270*, 419–426.
- (27) Thanthiripalage, K. S.; Nalin de Silva, K. *J. Mol. Struct. (THEOCHEM)* **2002**, *617*, 169–175.
- (28) Dreuw, A.; Head-Gordon, M. *Chem. Rev.* **2005**, *105*, 4009–4037.
- (29) Improta, R.; Barone, V.; Scalmani, G.; Frisch, M. J. *J. Chem. Phys.* **2006**, *125*, 054103.
- (30) Miertus, S.; Scrocco, E.; Tomasi, J. *Chem. Phys.* **1981**, *55*, 117–129.
- (31) Glendening, E.; Reed, A.; Carpenter, J.; Weinhold, F. NBO; University of Wisconsin: Madison, WI, 1998.
- (32) Reed, A. E.; Curtiss, L. A.; Weinhold, F. *Chem. Rev.* **1988**, *88*, 899–926.
- (33) Biegler-König, F.; Schönbohm, J.; Bayles, D. *J. Comput. Chem.* **2001**, *22*, 545–559.
- (34) Johnson, E. R.; Keinan, S.; Mori-Sánchez, P.; Contreras-García, J.; Cohen, A. J.; Yang, W. *J. Am. Chem. Soc.* **2010**, *132*, 6498–6506.
- (35) Frisch, M. J.; Trucks, G. W.; Schlegel, H. B.; Scuseria, G. E.; Robb, M. A.; Cheeseman, J. R.; Scalmani, G.; Barone, V.; Mennucci, B.; Petersson, G. A.; Nakatsuji, H.; et al. *Gaussian 09*, revision B.01; Gaussian, Inc.: Wallingford, CT, 2009.
- (36) Tenderholz, A. L. *QMForge, Version 2.1*; Stanford University: Stanford, CA, 2007.
- (37) Lu, H.; Yson, R.; Li, X.; Larochelle, C.; Patterson, H. H. *J. Phys. Chem. C* **2009**, *113*, 5952–5959.
- (38) Balanay, M. P.; Kim, D. H. *J. Phys. Chem. C* **2011**, *115*, 19424–19430.
- (39) Ma, R.; Guo, P.; Yang, L.; Guo, L.; Zhang, X.; Nazeeruddin, M. K.; Grätzel, M. *J. Phys. Chem. A* **2010**, *114*, 1973–1979.
- (40) Kleinman, D. *Phys. Rev.* **1962**, *126*, 1977–1979.
- (41) Yu, J.; Zerner, M. C. *J. Chem. Phys.* **1994**, *100*, 7487–7494.
- (42) Cammi, R.; Mennucci, B.; Tomasi, J. *J. Am. Chem. Soc.* **1998**, *120*, 8834–8847.
- (43) Yamaguchi, Y.; Yokomichi, Y.; Yokoyama, S.; Mashiko, S. *J. Mol. Struct. (THEOCHEM)* **2002**, *578*, 35–45.
- (44) Islam, M. M.; Bhuiyan, M. D. H.; Bredow, T.; Try, A. C. *Comput. Theor. Chem.* **2011**, *967*, 165–170.
- (45) Kulhánek, J.; Bureš, F.; Wojciechowski, A.; Makowska-Janusik, M.; Gondek, E.; Kityk, I. *J. Phys. Chem. A* **2010**, *114*, 9440–9446.
- (46) Aikens, C. M.; Li, S.; Schatz, G. C. *J. Phys. Chem. C* **2008**, *112*, 11272–11279.
- (47) Makowska-Janusik, M.; Kityk, I. V.; Kulhanek, J.; Bures, F. *J. Phys. Chem. A* **2011**, *115*, 12251–12258.
- (48) Gross, E.; Kohn, W. *Adv. Quantum Chem.* **1990**, *21*, 255–291.
- (49) Pedone, A.; Bloino, J.; Monti, S.; Prampolini, G.; Barone, V. *Phys. Chem. Chem. Phys.* **2009**, *12*, 1000–1006.
- (50) Barone, V.; Bloino, J.; Monti, S.; Pedone, A.; Prampolini, G. *Phys. Chem. Chem. Phys.* **2010**, *12*, 10550–10561.

- (S1) Contreras-García, J.; Johnson, E. R.; Keinan, S.; Chaudret, R.; Piquemal, J. P.; Beratan, D. N.; Yang, W. *J. Chem. Theory Comput.* **2011**, *7*, 625–632.
- (S2) Bader, R. F. W. *Atoms in Molecules – A Quantum Theory*; Oxford University Press: New York, 1990.
- (S3) Bader, R. F. W. *Acc. Chem. Res.* **1985**, *18*, 9–15.
- (S4) Bader, R. F. W. *Chem. Rev.* **1991**, *91*, 893–928.
- (S5) Bader, R. *J. Phys. Chem. A* **1998**, *102*, 7314–7323.